Orientation Factor in Steady-State and Time-Resolved Resonance Energy Transfer Measurements†

Pengguang Wu and Ludwig Brand*

Department of Biology, Johns Hopkins University, Baltimore, Maryland 21218

Received April 1, 1992; Revised Manuscript Received June 5, 1992

ABSTRACT: Resonance energy transfer measurements provide a way to estimate distances between chromophores attached to different sites of macromolecules. There are two unknowns involved in resonance energy transfer measurements, the distance between two chromophores and their relative orientation. When static orientational disorder exists, the orientation factor, κ^2, can vary from 0 to 4, leading to considerable uncertainty in estimation of distances. Fluorescence polarization anisotropy measurements can reduce the degree of uncertainty [Dale & Eisinger (1974) *Biopolymers 13*, 1573]. There may still be substantial error bounds for the average distance measurements. Time-resolved fluorescence measurements provide an "apparent" average distance and distance distribution containing contributions by both distance and orientation. The contribution of orientation to observed "apparent" average distance and distance distribution widths has been estimated for both simulated and real data. With a single unique distance as input in the simulation and with random but static orientation of donor and acceptor, the recovered average distance is very close to that of the input when the input distance is close to or larger than the Förster distance. The recovered width of apparent distance distribution can be substantial and it changes as a function of Förster distance to average distance ratio and as a function of Förster distance. Similar conclusions apply to the case where there is a real distance distribution. Motional averaging of the orientation was simulated by the Monte Carlo method to estimate the contribution of orientation when chromophores have certain degrees of mobility. As long as there is an apparent distance distribution, be it from angular or real distance distribution or from slow motions, the average distance may be obtained reliably provided the average distance is close to or greater than the Förster distance. The distribution can be measured by time-resolved fluorescence decay studies. When static orientation dominates, the shape of the "apparent" distribution fit depends on Förster distance to average distance ratio. A real distance distribution should have no such dependence.

Resonance energy transfer methods have been used to study molecular systems and large assemblies since the 1960s. Several reviews have dealt with different aspects in the application of this method (Stryer, 1978; Fairclough & Cantor, 1978; Steiner, 1990; Cheung, 1991; Eftink, 1991). Factors that may affect energy transfer rates have been extensively tested. Despite these efforts, several uncertainties remain. The most important one is perhaps the orientation factor of donor and acceptor in the estimation of average distances (Dale & Eisinger, 1974). Earlier work generally focused on the uncertainties of average distance between donor and acceptor arising from the uncertainties in the average value of the orientation factor κ^2 (Dale & Eisinger, 1974; Hillel & Wu, 1976; Haas et al., 1978; Dale et al., 1979) except that Haas et al. also estimated orientational contribution to the distance distribution of oligopeptide samples. The use of fluorescence polarization anisotropy results help to reduce the uncertainties of κ^2 to some degree (Dale et al., 1979). But it still leaves substantial error bounds for average distance calculation. In some cases, the anisotropy itself may not reveal complete information as to how the chromophores orient. For example, a complete static but random donor–acceptor pair and a static but unique configuration of donor–acceptor pair will both give $\kappa^2_{min} = 0$ and $\kappa^2_{max} = 4$, yet the distribution of κ^2 will be totally different. The increasing use of resonance energy transfer methods in the structural characterization of biological molecules makes it important to better understand the uncertainties associated with the measurements and interpretation. With the use of time-resolved resonance energy transfer method in the study of conformational heterogeneity and dynamics of many systems (Haas et al., 1975, 1978; Lakowicz et al., 1988; Cheung et al., 1991), the orientation factor will inevitably be an issue in interpreting experimental results. It is important to note that resonance energy transfer is dipolar in nature and the transfer rate depends on both distance separation and mutual orientation between chromophores. When experimental data are analyzed to obtain average distances or distance distributions with a single averaged value of orientation factor, the results are "apparent" ones which may or may not contain large contributions from orientational heterogeneity. It is the potential presence of static orientation that produced the much-discussed uncertainty associated with this method. Here we address the problem of orientation factor by both simulated and experimental data and show that by combining steady state with time-resolved measurements, the average distance between donor and acceptor (which is in many cases the most important parameter) can be reliably obtained without the uncertainties posed by the limits of orientation factor from anisotropy measurements alone. We further show that real distance distribution and orientation distribution in some cases have different characteristics in terms of their dependence on the Förster distance and it may be possible to differentiate between the two.

The paper is organized as follows. In the first section, we show simulated results on steady-state resonance energy transfer. In the second section, we simulate time-resolved

† This work was supported by National Institutes of Health Grant GM-11632 and by National Science Foundation Grant DIR-8721059.

0006-2960/92/0431-7939$03.00/0

data with a single distance as input to assess the contribution from orientation in terms of fitted apparent distance distribution width and average distance. In the third section, we simulate time-resolved data with a distance distribution to estimate the contribution from orientation. In the fourth section, the motions of chromophores are considered and simulated by Monte Carlo methods to address the narrowing down of orientation distribution. In the fifth section, we label a single site of a staphylococcal nuclease mutant to 100% with an acceptor with essentially no linker arm to check the existence of static orientational contribution to the observed distance distribution. We hope our results may help to reduce some unrealistic uncertainties associated with the estimation of average distance by the resonance energy transfer method, provide some guidelines in the interpretation of time-resolved results, and stimulate further research in conformational disorder in proteins and other macromolecular systems by time-resolved resonance energy transfer measurements.

MATERIALS AND METHODS

Simulated decay data in the presence of static orientational disorder were generated as follows. For a given situation, as will be shown in the next sections, a decay curve was generated for all possible configurations. The decay curve was then convoluted with an excitation function. Poisson noise was added to the convoluted curve to produce data that mimic an experimental decay curve. All simulations and data analysis were performed on an HP9000-835 computer.

The motions of donor or acceptor were simulated as follows. The donor and acceptor are assumed to have isotropic rotational diffusion constants D_d and D_a. Each can diffuse randomly. The trajectories of donor and acceptor were simulated by known Monte Carlo procedures (Ermak & McCammon, 1978; Martinez & Garcia de la Torre, 1987). The random variables R_i were generated such that $\langle R_\alpha \rangle = 0$ and $\langle R_\alpha^2 \rangle = 2D_\alpha t$, where α = a or d. The time step for steady-state results was chosen arbitrarily. For time-resolved decay, the time step was chosen to be much smaller than the experimental sampling time so that a stable average was obtained in the simulation. For each randomly generated configuration, the donor or acceptor was allowed to randomly jump to a new orientation with the constraint of overall donor or acceptor distribution. The orientation factor was then calculated and averaged. The random process went on until the time had reached an experimental sampling time interval. The decay intensity at that sampling time interval was then calculated from the partially averaged orientation factor.

The purification of staphylococcal nuclease mutant K78C (mutant kindly provided by D. Shortle, Johns Hopkins University) is described elsewhere (James, Wu, Stites, and Brand, submitted). The protein in monomer and cystine dimer forms was dissolved in 6 M GuHCl, 0.1 M Tris, and 0.05 M NaCl, pH 7.8. The dimer was reduced by adding excess dithiothreitol (DTT). The solution was either heated to 60 °C for 2 h or kept at room temperature overnight under argon. The reduced sample was passed though a Pharmacia PD-10 gel-filtration column to eliminate most of the reducing reagent. Excessive DTNB [5,5′-dithiobis(2-nitrobenzoic acid)] was added. The solution was stirred at room temperature for 2 h and shielded from light. After a dialysis and concentration step, the sample was purified by HPLC gel filtration (Bio-Rad SEC-125 column). The fraction corresponding to the monomer was pooled and concentrated. The final buffer was 0.1 M Tris, 0.05 M NaCl, and 1 mM EDTA, pH 7.5. The TNB to protein ratio was determined both by the absorption of TNB covalently attached to the nuclease and by that of the released TNB in the presence of 10-fold DTT. The latter procedure is one of the ways to carry out DTNB titration where the absorption of TNB ion at 412 nm (ϵ_{412}) = 14 150 M^{-1} cm^{-1} (Riddles et al., 1979) is used. We found 1 mol of TNB/mol of protein. Thus the protein was 100% labeled with TNB.

Time-resolved fluoresence decays of donor tryptophan in the absence and presence of acceptor TNB were collected with a picosecond synch-pump dye laser system and a time-correlated single photon counting apparatus as described earlier (Badea & Brand, 1979; Wu et al., 1991). The overall system response was about 60–70 ps. Triplicate data sets were collected at 20 °C.

Both simulated and experimental data were analyzed by nonlinear least-squares methods with the appropriate model functions described in the next few sections.

RESULTS

Steady-State Energy Transfer

In this section, we calculate steady-state transfer efficiency with a single distance and a random but static orientation as input in the simulation. Suppose in a coordinate system the donor is oriented at θ_d (polar angle), ϕ_d (azimuthal angle) and the acceptor at θ_a, ϕ_a; the orientation factor κ^2 can be written as

$$\kappa^2 = (\sin\theta_a \sin\theta_d \cos(\phi_a - \phi_d) - 2\cos\theta_a \cos\theta_d)^2$$

Assuming there is a single distance between the donor and acceptor, r, the steady-state energy transfer efficiency for a static and random system is

$$\bar{E} = \frac{1}{16\pi^2}\int\int\int\int \frac{(R'_0/r)^6\kappa^2}{1 + (R'_0/r)^6\kappa^2} \sin\theta_a \sin\theta_d \, d\phi_a \, d\phi_d \, d\theta_a \, d\theta_d \quad (1)$$

where R'_0 is the Förster distance without the averaged κ^2, i.e., $R'^6_0 \langle\kappa^2\rangle = R_0^6$. As Dale and Eisinger (1974) pointed out, the average transfer efficiency has an equivalent average orientation factor that depends on distance.

Equation 1 can be rewritten as

$$\bar{E} = \frac{1}{16\pi^2}\int E \, d\phi_a \, d\phi_d \, d\theta_a \, d\theta_d \quad (2)$$

where E is a function of all four angular variables and the distance between chromophores. We calculate the distribution of E by sampling all possible orientations for a fixed distance. The distribution of transfer efficiency E arising from static orientation is shown in Figure 1 for R_0/r ratio fixed at 0.64, 0.94, and 1.37. The distribution of transfer efficiency, primarily from distribution of κ^2 as has been calculated by others (Dale et al., 1979; Haas et al., 1978), will ultimately determine how the apparent distance distribution looks when a single orientation factor is used in the data analysis of time-resolved decay curves. The discontinuity in the distribution of E is due to that in κ^2 distribution which has been shown earlier (Dale et al., 1979; Haas et al., 1978). At all three distance ratios, the distribution of E is heavily skewed to small values. In other words, there are many orientations in the random but static configuration where little energy transfer occurs. The shape of the distribution of E changes as a function of R_0/r. At $R_0 > r$, the distribution is very wide, covering the entire range. At $R_0 < r$, it is substantially smaller. This is due to the nature of dipolar interaction. When two chro-

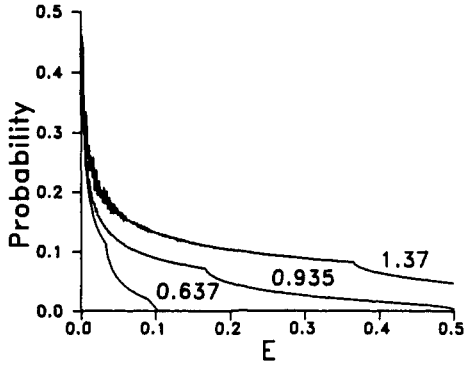

FIGURE 1: Distribution of energy transfer efficiency due to random and static orientation of donor and acceptor. The probability of E was calculated according to eqs 1 and 2 with all possible orientations of donor and acceptor for a given distance. The three curves were calculated for three Förster distance to input distance ratios.

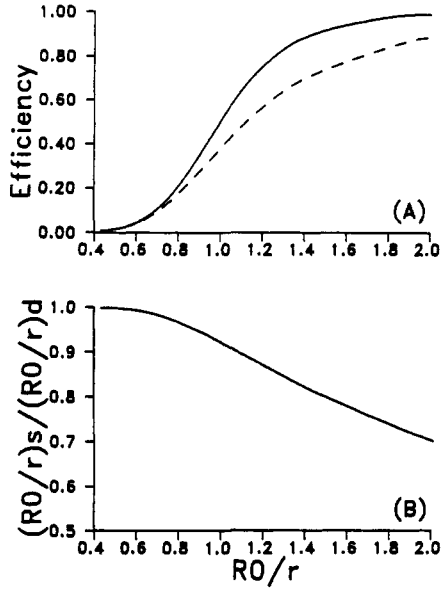

FIGURE 2: (A) Energy transfer efficiency as a function of Förster to average distance ratio in the case of dynamic (solid line) and static orientation (dashed line). (B) Deviation of calculated average distance using orientation factor $^2/_3$ in the case of random and static orientation of donor and acceptor.

mophores are far away, the mutual orientation is not as important as when they are close.

The average transfer efficiency as a function of R_0/r is shown in Figure 2A for dynamic ($\kappa^2 = {}^2/_3$) and static but random orientation. Compared to the case of dynamic averaged orientation factor, static orientation reduces the overall energy transfer efficiency as can be predicted from the efficiency distributions in Figure 1.

Our interest is to find out how serious the error is due to static but random orientation. This is shown in Figure 2B. The input in the calculation of average transfer efficiency is the ratio R'_0/r. The dynamic average value is then $(R_0/r)_d^6 = (R'_0/r)^6\langle\kappa^2\rangle$ with $\langle\kappa^2\rangle = {}^2/_3$. After the static but random orientation is superimposed as in eq 1, the average transfer efficiency is obtained. This represents "measured" transfer efficiency. Next, $(R_0/r)_s$ is calculated from

$$\bar{E} = \frac{(R'_0/r)_s^6\langle\kappa^2\rangle}{(R'_0/r)_s^6\langle\kappa^2\rangle + 1}$$

using $\langle\kappa^2\rangle = {}^2/_3$. Thus $(R_0/r)_s = (R'_0/r)_s\langle\kappa^2\rangle^{1/6}$ represents the average distance calculation from the "measured" transfer efficiency. In the absence of static orientation, $(R_0/r)_s$ would be exactly equal to $(R_0/r)_d$ and $(R_0/r)_s/(R_0/r)_d = 1.0$. Deviation from 1.0 reflects the error introduced by static orientation. Figure 2B shows that when $R_0 > r$, the error is large, but when $R_0 < r$, the error is small. Thus, in terms of average distance between chromophores, a static but random orientation may not necessarily introduce large errors when the system is chosen such that $R_0 < r$, which is often the case in various measurements. It should be noted that if r is much larger than R_0, errors in the measurements of energy transfer efficiency will increase.

In real systems, it is very likely that we do not know the distribution of orientations. Fluorescence polarization anisotropy measurements may be useful to narrow down the range of κ^2 to a certain degree. They still leave substantial uncertainties because only the bounds, not the distributions, of κ^2 are estimated. On the other hand, time-resolved energy transfer measurements can be used to further reduce the uncertainties associated with the estimation of average distances.

Static Orientation with a Single Distance

In this section we ask how a static orientation can contribute to an observed width of "apparent" distance distribution when a single average value for the orientation factor is used in data analysis of time-resolved resonance energy transfer measurements.

(1) Both Donor and Acceptor Are Static and Random. Suppose a situation exists where there is a fixed distance between a donor and an acceptor but a random but static distribution of orientations. If the orientation is static on the nanosecond time scale, emission anisotropy measurements would not indicate rotational motion and κ^2 could have values between 0 and 4. What conclusions would be reached from time-resolved measurements with analysis in terms of a $\kappa^2 = {}^2/_3$? In this case, the fluorescence decay of the donor can be expressed as

$$I(t) = \alpha\int\int\int\int\exp\left[-\frac{t}{\tau}(1 + (R'_0/r)^6\kappa^2)\right]\sin\theta_a\sin\theta_d\,d\phi_a\,d\phi_d\,d\theta_a\,d\theta_d \quad (3)$$

where α is the amplitude and τ is the donor lifetime in the absence of acceptor.

The simulated data were generated as follows. $I(t)$ was calculated for all possible orientations at each time point (out of a total of 1024 data points in time). It was then convoluted with an excitation function. Poisson noise was added afterwards.

The simulated data were analyzed by

$$I(t) = \int p(r)\exp\left[-\frac{t}{\tau}(1 + (R_0/r)^6)\right]dr \quad (4)$$

where R_0 was calculated using the orientation factor $^2/_3$. The apparent distance distribution $p(r)$ was assumed to be either a Gaussian function

$$p(r) = \frac{1}{(2\sigma\pi)^{1/2}}\exp\left[-\frac{1}{2}\left(\frac{r-\bar{r}}{\sigma}\right)^2\right] \quad (5)$$

or a Lorentzian function

$$p(r) = \frac{1}{\sigma\pi}\left[1 + \left(\frac{r-\bar{r}}{\sigma}\right)^2\right]^{-1} \quad (6)$$

where σ is the standard deviation of the distribution and $\bar{r}$ is the mean distance.

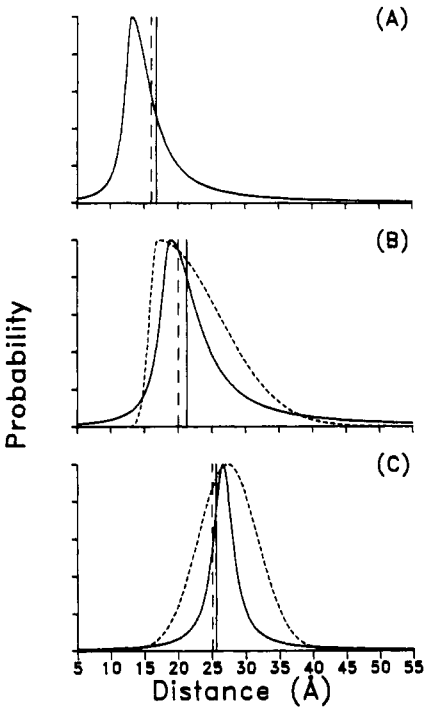

FIGURE 3: Apparent distance distributions obtained from fits to decay data generated using a single distance input at 16 Å (A), 20 Å (B), and 25 Å (C) and random but static orientation of donor and acceptor in the simulation. The Förster distance was 18.69 Å. The vertical dashed line is the input distance while the vertical solid line is the average distance from the data analysis. The solid curve is the Lorentzian fit to the decay data while the dashed curve is the Gaussian fit. In (A) no Gaussian could fit the decay data. The position of average distance over distance distribution changes due to the nonlinear weighting of probability in energy transfer.

In addition, skewed Gaussian or Lorentzian functions were also used. The skew is defined by a parameter s:

$$\sigma_L = 2\sigma/[1 + \exp(s)]$$

$$\sigma_R = 2\sigma \exp(s)/[1 + \exp(s)]$$

where σ_L and σ_R are the standard deviations of the left and right sides of the distribution.

$I(t)$ was calculated from eq 4 and convoluted with an excitation function and compared with eq 3 by a nonlinear least-squares method. The results are shown in Figure 3 where the input for simulation was: $\tau = 5$ ns, $R'_0 = 20$ Å ($R_0 = 18.69$ Å), and r = 16, 20, and 25 Å. Additional results are shown in Table I.

Three aspects emerge from this simulation experiment. (1) The average distance obtained from analysis of the simulated data is very close to that used for the simulation. The errors in average distance do not exceed more than 10%. (2) At shorter distances, when $R_0 > r$ only skewed functions could fit the data. Only at $R_0 < r$ was it possible for the simulated data to be fit with either a symmetric Gaussian or a Lorentzian. In summary the noticeable feature of the apparent distance distribution is that as the ratio R_0/r changes, the peak and shape of the fitted distribution change as well. Since it might be possible to change R_0 by quenching the donor, this might be a useful diagnostic tool for energy transfer studies. (3) With a single distance as input in the simulation, an "apparent" distance distribution could be observed. For example, the observed full width at half maximum of distance distribution fit was 12 Å with $R_0 = 18.7$ Å.

The width of the "apparent" distribution fit due to static orientation is expected to be larger for larger R_0. We checked this by simulation with larger values of R_0. The results are shown in Figure 4. The apparent σ of a Gaussian fit scales with R_0. The ratio σ/R_0 was found to be 0.27. For example, the apparent σ at $R_0 = 18.7$ is 5.1 Å, and at $R_0 = 56.1$ Å it is 15.2 Å, which corresponds to a full width at half maximum of an apparent distance distribution of about 35 Å. Thus static orientation makes a larger contribution in absolute value to the observed width of distribution fit at larger Förster distances.

(2) *One Chromophore Is Random and Static and the Other One Is at a Unique Orientation.* For simplicity, we set for example $\phi_d = 0$ and choose $\theta_d = 0$, 45°, and 90°. The simulation was similar to eq 3 except one chromophore was set at a unique orientation. The results are shown in Table II. Although the orientation of one chromophore is unique, the presence of another random statically oriented chromophore leads to a similar "apparent" distribution width compared to the case where both are random. The overall average distance is no more than 15% off from the input value in the worst case. It thus appears that as long as there is a distribution of angular orientations, be it from a single chromophore or from both, it will lead to a certain distribution width in the fit but not much error in the average distance.

Orientational Contribution with Distance Distribution Present

The purpose here is to see how much the orientation factor can contribute to the observed average distance and width of the apparent distance distribution fit when there is a real distance distribution. The equation used to simulate the decay is

$$I(t) = \int\int\int\int\int p_s(r) \exp\left[-\frac{t}{\tau}(1 + (R'_0/r)^6\kappa^2)\right] \sin\theta_a \sin\theta_d \, d\phi_a \, d\phi_d \, d\theta_a \, d\theta_d \, dr \quad (7)$$

where $p_s(r)$ is a true distance distribution. When eq 4 is used to analyze the simulated data, the apparent width is the combination of contributions from real distance distribution width and from static orientation.

The input distance distribution function was a Gaussian with $\sigma = 5.0$ Å and the average distance was chosen to cover the range smaller than R_0 to greater than R_0. The results are shown in Figure 5 for three distances. All parameters are summarized in Table III. As in the case of a single distance input, at $R_0 < r$, both a symmetric Gaussian and a Lorentzian fit the decay data. At $R_0 \geq r$, skewed apparent distance distribution functions are required to fit the data. The presence of a true distance distribution in the simulation does not change this pattern. Even though the shape of the input Gaussian is identical, the shape of the apparent distance distribution fit (mean, width, and skewness) changes as a function of Förster distance to mean distance ratio. This is again due to the nature of dipolar interactions between chromophores.

Compared to the case of a single distance, the contribution from static orientation to the observed apparent distance distribution width is not additive to the real distance distribution width. For example, with a single distance as input, $\sigma = 5.1$ Å was obtained for $R_0 = 18.69$ Å, while with the same distance as median distance of a Guassian distance distribution in the simulation, $\sigma = 7.9$ Å was obtained out of an input of a true distance distribution width 5.0 Å. A direct summation would lead to 10.1 Å in the width of the apparent distance

Table I: Fitting Parameters to a Single Distance and Random Orientation

input distance (Å)	$\bar{\tau}^a$ (ns)	Gaussian fit $\bar{r}$	Gaussian fit σ	Gaussian fit s	Lorentzian fit $\bar{r}$	Lorentzian fit σ	Lorentzian fit s	$r_{obs}{}^b$ (Å)
16	1.72	c	c	c	13.2	2.4	1.0	16.8
18	2.91	c	c	c	16.2	2.8	1.5	19.7
20	3.44	17.0	5.1	2	18.9	3.3	1.0	21.3
22	3.88	21.2	5.1	1.	21.0	3.2	1.0	23.0
25	4.35	27.4	4.4	0	26.6	1.8	0	25.6

[a] Average lifetime of the decay data obtained by multiexponential analysis. Donor lifetime in the absence of acceptor was 5 ns. [b] Observed average distance calculated from average lifetime. [c] No fit.

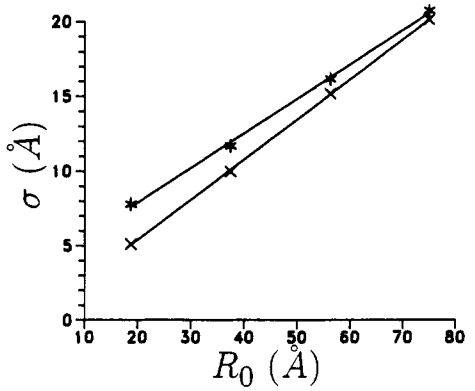

FIGURE 4: Width of apparent distance distribution fit to simulated data generated with random but static orientation and a single distance input (×) or a distance distribution (*) as a function of Förster distance R_0. The input distance was at R_0/r or $R_0/\bar{r} = 0.94$. In the case of distance distribution input a Gaussian was used with $\sigma = 5.0$ Å. The data were analyzed using an asymmetric Gaussian (skew = 2) in the case of single distance input and a symmetric Gaussian in the case of a distance distribution input.

Table II: Fitting Parameters When One Orientation Is Unique[a]

confign θ_d	Gaussian fit $\bar{r}$	Gaussian fit σ	Gaussian fit s	Lorentzian fit $\bar{r}$	Lorentzian fit σ	Lorentzian fit s	r_{obs} (Å)
0	b	b	b	15.5	2.4	2.0	19.4
45	b	b	b	16.7	2.6	2.0	20.5
90	22.9	4.3	0.5	21.4	2.7	1.0	23.2

[a] The distance input was 20 Å. [b] No fit.

distribution fit. Thus with a comparable distance distribution, the effects of static orientation may be reduced to some degree.

Since static contribution depends on Förster distance as we showed in the last section, the observed width here also contains a variable contribution from static orientation that increases with R_0. The results are shown in Figure 4. For an input of $\sigma = 5.0$ Å of a true Gaussian distance distribution as input in the simulation, a large part of the observed width is due to the real width at $R_0 = 18.7$ Å. On the other hand, this distance distribution input has almost no effect on the observed width when R_0 is larger than 60 Å. For example, at $R_0 = 75$ Å, which probably is close to the experimental upper limit of a donor–acceptor pair, the apparent width from static orientation is the same when either a single distance or a Gaussian distance distribution with $\sigma = 5$ Å was used as input in the simulation.

Motion Averaging of Orientation

Molecules in solution can undergo thermal Brownian motion. The angular rotations of donor or acceptor tend to narrow down the distribution of orientations. Angular distribution contributes to different transfer rates because the term κ^2 in eqs 3 and 7 depends on four angular variables

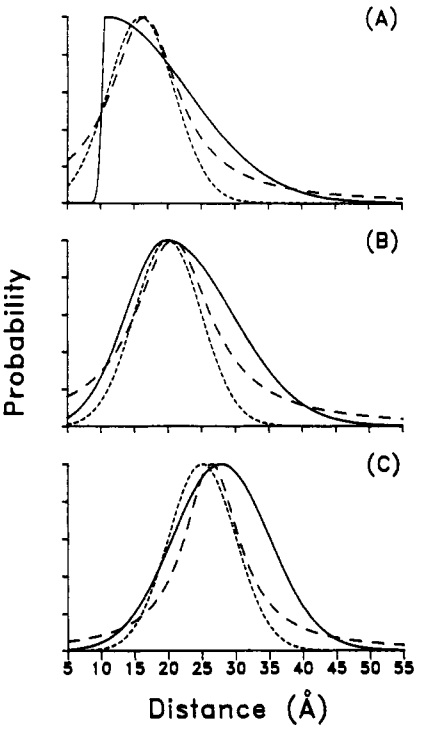

FIGURE 5: Apparent distance distributions obtained from fits to decay data generated using a Gaussian distance distribution (short dashed line) with $\sigma = 5.0$ Å and median distance at 16 Å (A), 20 Å (B), and 25 Å (C) and static but random orientation of donor and acceptor in the simulation. Gaussian (solid line) and Lorentzian (long dashed line) fits are also shown. Input Förster distance was 18.69 Å.

Table III: Fitting Parameters with a Distance Distribution

median distance[a]	$\bar{\tau}^b$ (ns)	Gaussian fit $\bar{r}$	Gaussian fit σ	Gaussian fit s	Lorentzian fit $\bar{r}$	Lorentzian fit σ	Lorentzian fit s	$r_{obs}{}^c$ (Å)
16	2.38	10.8	6.2	3.0	16.5	6.3	0	18.3
18	2.87	15.8	7.4	1	18.4	6.8	0	19.6
20	3.29	19.7	7.9	0.5	20.7	6.9	0	20.8
22	3.65	22.0	7.8	1	21.1	6.6	0	22.1
25	4.13	27.8	7.2	0	26.4	5.0	0	24.2

[a] Input mean distance of a Gaussian distance distribution with $\sigma = 5$ Å. [b] Average lifetime. [c] Observed average distance calculated from average lifetime.

in the static regime. In the dynamic regime where molecules undergo faster reorientation compared to energy transfer rate, κ^2 will take an average value regardless of where the initial or final orientations are. In the intermediate regime where orientation rate is comparable with energy trasnfer rate, κ^2 is only partially averaged so that it still has some degree of dependence on the orientations of the molecules. This can be addressed by simulating the motions of donor and acceptor.

The simulation was checked with steady-state results. With $D_d = D_a = 1 \times 10^{11}$ s^{-1} and 10^5 simulations, the average transfer efficiency for $R'_0 = 20$ Å ($R_0 = 18.69$ Å) and $r = 20$ Å is 0.4002 compared to the exact value of 0.4000. The overall $\langle\kappa^2\rangle = 0.6672$ compared to the exact value of 0.6667.

The time scale of motions that can reduce orientational effects in donor and acceptor relative to energy transfer rate becomes clear if we compare the time-resolved decay data. For simplicity, we first assume that both donor and acceptor have the same diffusion constants. Figure 6 shows the apparent σ of a Gaussian distribution fit to the simulated data using a true Gaussian distance distribution with $\bar{r} = 20$ Å and $\sigma = 5.0$ Å as input. At low diffusion constants, the results are essentially the same as those of random static orientation (Figure 5). As the diffusion rate goes up, the fitted σ gradually

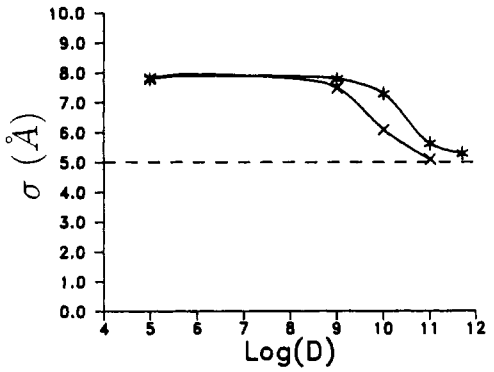

FIGURE 6: Reduction of orientation effects due to motions of chromophores. The apparent width σ was obtained using a Gaussian function in the fit. The input in the simulation was a Gaussian distance distribution with $\sigma = 5.0$ Å. In the case of mobile donor and acceptor (×), the diffusion constants of both were set equal. In the case of one mobile chromophore (*), the diffusion constant of the rigid one was set at 1×10^5 s^{-1}. The x-axis plots the logarithm of the diffusion constant of the mobile chromophore(s).

reduces to the true value. Here we used the donor lifetime of 5 ns in the simulation. The transfer rate at the median distance is about 2.5 ns^{-1}. The diffusion constant required to achieve dynamic averaging is of the order 10^{11} s^{-1}, or 100 ns^{-1}, which corresponds to a few picoseconds in correlation time of donor or acceptor.

In some cases, it might be possible that one chromophore is mobile while the other one is rigid. It is interesting to see how orientational effects contribute to the observed width in the fit. If one chromophore is static and random and the second one is totally dynamic, then the system is essentially close to the dynamic case. For a Gaussian input ($\bar{r} = 20$ Å, $\sigma = 5.0$ Å) in the simulation, the results are $\bar{r} = 20.3$ Å and $\sigma = 5.3$ Å. At lower diffusion constants, the contribution to the width is expected to be larger than the case where both chromophores are mobile. When one chromophore is immobile, the diffusion constant of the mobile one reduces the effects of orientation at a lower rate, as shown in Figure 6. As in the case of static orientation, the contribution from orientation is also reduced when there is a distance distribution present. For example, with $D = 10^{10}$ s^{-1} and a single distance of 20 Å as input in the simulation, the orientation from the chromophores can contribute to a width of apparent distance distribution fit of $\sigma = 3.8$ Å. With a Gaussian distance distribution $\bar{r} = 20$ Å and $\sigma = 5.0$ Å as input (data not shown), the fitted σ only rises to 6.8 Å instead of 8.8 Å.

Apparent Distance Distribution in a Staphylococcal Nuclease Mutant

The orientation effects were tested on a staphylococcal nuclease mutant K78C, where lysine-78 was replaced by cysteine. We used the single tryptophan at position 140 as the donor and labeled the SH group with DTNB. The use of TNB as an acceptor has several advantages. DTNB has been used in the titration of free SH groups in proteins (Ellman, 1959). The procedure for titration is well established and the quantitation of the percentage labeling is reliable. Since DTNB reacts with the SH group by disulfide exchange, the labeling is site specific. The reaction can easily reach 100% with a large excess of DTNB. This is important since one cannot differentiate between what is unlabeled and what are those configurations with little or no energy transfer. There are only two single bonds between the site of labeling and the acceptor chromophore, thus reducing some uncertainties due to the linker arm. The disadvantage is that DTNB does not fluoresce and behaves only as a quencher.

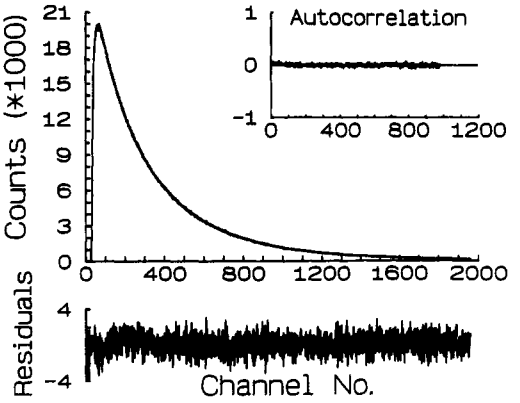

FIGURE 7: Measured and fitted decay curve of tryptophan fluorescence in staphylococcal nuclease mutant K78C labeled with TNB. Intensity is given as counts vs channel number as time base (0.0107 ns/channel). The weighted residuals and the autocorrelation of the residuals are also shown. The protein was in 0.1 M tris, 0.05 M NaCl, and 1 mM EDTA, pH 7.5. The excitation was at 295 nm and the emission at 350 nm. Temperature was set at 20 °C.

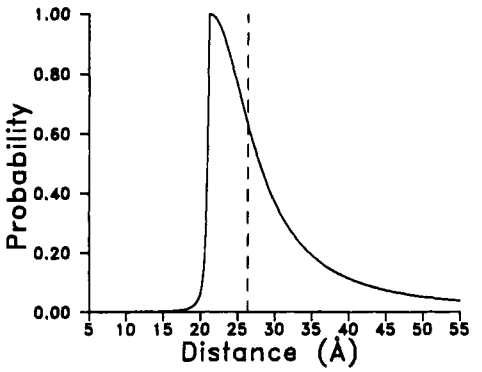

FIGURE 8: Apparent distance distribution obtained from fits in Figure 7. One skewed Lorentzian was used. The vertical dashed line is the average distance calculated from the average lifetime of the sample. Förster distance $R_0 = 24.1$ Å. Parameters of the fit: $\bar{r} = 22.2$ Å, $\sigma = 2.4$ Å, $s = 3$.

The decay data of tryptophan in the presence of TNB were analyzed using eq 4 as a fitting function to obtain the apparent distance distribution function $p(r)$ between Trp 140 and TNB at 78. The fits are shown in Figure 7. The fit to experimental data was judged by reduced-χ^2, plot of the residuals, and examination of the autocorrelation of the weighted residuals. We were unable to fit the decay curves with a symmetric function, either Gaussian or Lorentzian. In fact even an asymmetric Gaussian could not fit the decay data. Of the fitting functions tested, only an asymmetric Lorentzian fit the data and the distribution is shown in Figure 8. Clearly, the curve is largely skewed to the longer apparent distances. The average distance between Trp 140 and 78 can be estimated from crystallographic data to be about 23–25 Å. The average distance obtained here is 26.4 Å. Thus no matter what the distribution form is, the measured average distance reflects the overall dimension of the protein in the native state. On the other hand, even allowing for some degree of structural fluctuation in the native state, the apparent distances of some fraction of the molecules are too long. Since we labeled the protein to 100%, the labeled protein was stable in the dark for a few weeks, and we found no detectable decomposition after the measurements, the long tail of the apparent distance distribution is not due to the contribution from unlabeled or decomposed products. The enzymatic activity of the protein labeled with a larger molecule was found to be close to that of the unlabeled protein (James, Wu, Stites, and Brand, submitted) so that it is unlikely that a large fraction of the

protein here is denatured. Judging from Figures 1, 3, and 5, it is likely that the apparent presence of nuclease molecules with very large distances arises from the static orientation of the donor or acceptor or both.

DISCUSSION AND CONCLUSION

In this paper we presented simulated and experimental data to assess the contribution of orientation effects to the observed average donor–acceptor distance and the apparent width of distance distribution when static orientation is present. In light of the present results, we discuss several aspects in the implementation of energy transfer measurements and in the interpretation of experimental data. We will focus our discussion on average distance estimation and on distance distribution estimation.

Average Distance Estimation. The primary concern with orientation factor κ^2 in average distance determination results from the fact that κ^2 can vary from 0 to 4 and the average distance will be in error if the donor and acceptor adopt a unique orientation, with a κ^2 away from its average $^2/_3$ and immobile on the time scale of energy transfer. With fluorescence polarization anisotropy measurements the lower and upper limits of κ^2 may be estimated (Dale et al., 1979). But the average distance between chromophores is determined not by the limits of κ^2 but rather by the distribution of κ^2 even when there is no real distance distribution present. An additional complication is that it is not easy to define the motions of the chromophores themselves since many systems exhibit internal motions with comparable time scales. Although different types of donor–acceptor orientational distributions can potentially give the same limits of κ^2 from anisotropy results alone, they will lead to quite different apparent distance distributions in time-resolved energy transfer measurements. For example, if two chromophores are at a unique configuration, the system should produce no apparent distance distribution. Time-resolved energy transfer measurements provide more information for the characterization of donor–acceptor distances.

If orientation factor is the only factor that determines the observed apparent distance distribution, then the more constrained the two chromophores are, the narrower the apparent distance distribution is. On the other hand, if there is distance heterogeneity either due to macromolecular systems alone or due to linker arms of probes, or both, orientational freedom will certainly exist to a substantial degree. Our results show that with a donor–acceptor pair chosen such that the average distance is in the vicinity of or larger than the Förster distance, the average distance can be obtained reliably as long as there is an "apparent" distance distribution even though static orientational disorders might be present. The apparent distance distribution may be due to orientation distribution or real distance distribution from the system or it may be introduced by the linker arm (Haas et al., 1988). It should be noted that our simulations represent some of the worst cases where κ^2 can vary from 0 to 4. With a smaller range of κ^2, many authors have shown that average distance can be obtained without large uncertainty (Hillel & Wu, 1976; Stryer, 1978; Haas et al., 1978). Since extrinsic probes have been used in most of the systems studied so far, it is unlikely that a donor–acceptor pair orients at a unqiue configuration to produce a peculiar κ^2 value in solution. Thus the uncertainties deduced from anisotropy measurements alone may not be realized experimentally.

Of all the time-resolved results of donor acceptor pairs, only some oligopeptides (Haas et al., 1975), α-helical melittin (Lakowicz et al., 1990a), and some glycopeptides (Rice et al., 1991; Wu et al., 1991) show very narrow distance distribution width. In these cases, there are some constraints in the structure between the donor and acceptor while the chromophores at the ends are basically free to rotate. Most systems studied so far exhibit some apparent distance distributions (Haas et al., 1975, 1988; Amir & Haas, 1987; Lakowicz et al., 1988; Albaugh & Steiner, 1989; Cheung et al., 1991). Even in the native states of proteins, there is a substantial width in apparent distance distribution which probably reflects the fact that, in addition to possible protein conformational fluctuations, extrinsic probes with linker arms also make contributions. It should be noted that in these protein systems the average distances from resonance energy transfer measurements are very close to those known from other techniques such as X-ray (Amir & Haas, 1987; Haas et al., 1988). Similarly, in our case of staphylococcal nuclease, the average distance is very close to X-ray data even though there is an apparent distance distribution. Steady-state results also show that the average distances from energy transfer methods are correct (Hahn & Hammes, 1978) with uncertainties much smaller than those posed by the limits of κ^2. Thus even without knowledge of the exact source of the large apparent distance distribution, the overall dimensions of proteins and other molecular systems can be obtained reliably just as in the case of model compounds (Conrad & Brand, 1968; Stryer, 1978).

Distance Distribution Estimation. The apparent distance distribution from time-resolved resonance energy transfer measurements contains several contributions as discussed earlier. Whereas the use of donor–acceptor pairs with Förster distance close to or smaller than the average distance produce more reliable results in the average distance estimation alone, donor–acceptor pairs with Förster distances close to or larger than the average distance are more suitable for shape information of an "apparent" distance distribution. Ideally we would like to measure conformational heterogeneity of proteins and other macromolecular systems and be able to differentiate distance from orientational heterogeneity. However, additional factors have to be considered when extrinsic probes are used. In the following, we discuss several situations.

(A) Both Donor and Acceptor Are Intrinsic Probes or Minor Modifications of Them. Many proteins have intrinsic chromophores such as tryptophan and tyrosine which may be used directly or with minor modifications. In addition, some proteins have tightly bound ligands that may be used as chromophores. In these cases, both distance and orientational heterogeneity reflect the conformational fluctuations of the proteins in solution where they are subject to thermal fluctuations, especially on the surfaces. A static orientational disorder may exist without a distance distribution. But the presence of a distance distribution will be certain to lead to an orientational disorder. Our results show that the presence of a static orientational disorder can produce a wide apparent distance distribution but the shape is generally skewed to apparent donor–acceptor distances that are physically impossible to be within the native state of proteins. Furthermore, one can quench the donor to observe changes in the shape of apparent distance distributions. A change of shape also means there is a substantial orientational disorder since a real distance distribution should not depend on Förster distance. One important factor that can be used to probe structural fluctuations is temperature. But care must be taken in the interpretation of experimental results. While distance disorder

may decrease with decreasing temperature, orientational disorder may increase.

With the advancement of protein engineering and molecular biology, it is possible to produce many proteins with desirable spectroscopic characteristics. Site-directed incorporation of a particular chromophore into proteins (Ellman et al., 1992) should greatly facilitate the use of resonance energy transfer methods in the studies of protein conformations in solution. Steiner et al. (1991) used an engineered calmodulin to study the distance distribution of the protein in the native state. The Förster distance was much larger than the average distance so that their distance distribution shape should be defined well experimentally. From our results it is clear that the existence of a large orientational disorder would skew their apparent distribution shape, which is not the case. This is consistent with their conclusion that the distribution is mainly from distance heterogeneity. One interesting feature to notice is that the limit of κ^2 from their anisotropy should be quite large since both chromophores are quite immobile and yet the average distance they obtained is quite close to that from X-ray data.

Protein–protein interactions can also be studied by distance distribution. If one subunit contains one chromophore and another subunit a different chromophore, time-resolved resonance energy transfer measurements provide a unique means to study the interaction which is not covalent in nature and is subject to much larger thermal fluctuations in solution or in membranes. With chromophores confined to some limited configurations, both distance and orientational information can be obtained between the two interacting subunits.

(*B*) *One or More Probes Are Extrinsic.* In most cases, one or more extrinsic probes are used in resonance energy transfer measurements. The introduction of extrinsic probes may complicate the interpretation of apparent distance distribution in a sense that their own linker arms can potentially contribute to distance or orientational heterogeneity. However, depending on the problems one is interested in, useful and unique insights about the conformations of molecular systems in solution can be obtained. In the case of random coils or structureless biopolymers in solution, local or global motions tend to randomize the orientations of the probes on the time scale of measurements so that the apparent distance distribution is due to conformational heterogeneity or diffusion (Haas et al., 1975; Lakowicz et al., 1990b). Another case where linker arms are unimportant is the use of apparent distance distribution in determining large-scale multiconformers of macromolecular systems in solution. These conformers are otherwise difficult to determine by other techniques due to either heterogeneity or fast interconversion. Recently we have determined flexibilities of branching complex carbohydrates which are prevalent in many glycoproteins (Rice et al., 1991; Wu et al., 1991).

Protein structure and protein–protein interactions are important problems in structural biology. While X-ray or NMR methods provide high-resolution structures of proteins in the native states, the structures are time-averaged. In solution where proteins are subject to thermal fluctuations, structural heterogeneity, either local or global, can occur on various time scales. Time-resolved resonance energy transfer measurements can capture most of the fluctuations. The use of extrinsic probes may complicate the results since many commercially available probes are produced with long linker arms. Substantial improvements in the spectroscopic characteristics of these probes are needed to obtain more detailed structural information of small globular proteins in the native states. However, for subunit–subunit or protein–protein interactions, resonance energy transfer methods are useful, as has been demonstrated by numerous examples in the literature. In many cases, one is more interested in the change of a conformation rather than the conformation itself, and the distance distribution approach, even with extrinsic probes, can extend to many complex systems that are beyond the reach of other methods.

Protein denaturation studies provide useful information in the understanding of protein stability and folding. Although many proteins denature in a two-state manner thermodynamically, structural information during and immediately after the denaturation of proteins is very limited. Under conditions where proteins are destabilized, the degree of heterogeneity in protein structures is much larger than that from the linker arms so that the introduction of extrinsic probes poses no significant problems in the study of these complex systems. The distance distribution approach can thus lead to structural insights about the gross conformations of the denatured states of proteins in solution under different conditions such as temperature, pH, and denaturants.

No matter whether the probes are intrinsic or extrinsic, if orientational contribution is the dominant factor that determines an apparent distance distribution, then the distribution fit from data analysis will be skewed to longer apparent distances. Since a distance distribution shape should not depend on R_0 while a distribution containing a large orientational distribution does, two approaches can be used. One approach is to choose a donor–acceptor pair such that $R_0 > r$; then by quenching the donor, one reduces R_0. Another approach is to select a series of pairs with increasing R_0 but similar structures. While average distances can be obtained reliably when the Förster distance is shorter than the average distances, the shape distribution is better defined when the Förster distance is longer. This is true for either an orientation distribution or a distance distribution. Thus it may be possible to better define the nature of distribution fit.

REFERENCES

Albaugh, S., & Steiner, R. F. (1989) *J. Phys. Chem. 93*, 8013–8016.

Amir, D., & Haas, E. (1987) *Biochemistry 26*, 2162–2175.

Badea, M., & Brand, L. (1979) *Methods Enzymol. 61*, 378–425.

Cheung, H. C. (1991) in *Topics in Fluorescence Spectroscopy, Vol. 2, Principles* (Lakowicz, J. R., Ed.) pp 127–176, Plenum Press, New York.

Cheung, H. C., Gryczynski, I., Malak, H., Wiczk, W., Johnson, M. L., & Lakowicz, J. R. (1991) *Biophys. Chem. 40*, 1–17.

Conrad, R. H., & Brand, L. (1968) *Biochemistry 7*, 777–787.

Dale, R. E., & Eisinger, J. (1974) *Biopolymers 13*, 1573–1605.

Dale, R. E., Eisinger, J., & Blumberg, W. E. (1979) *Biophys. J. 26*, 161–194.

Eftink, M. R. (1991) in *Methods of Biochemical Analysis* (Suelter, C. H., Ed.) Vol. 35, pp 129–205, John Wiley & Sons, Inc., New York.

Ellman, G. L. (1959) *Arch. Biochem. Biophys. 82*, 70–77.

Ellman, J. A., Mendel, D., & Schultz, P. G. (1992) *Science 255*, 197–200.

Ermak, D. L., & McCammon, J. A. (1978) *J. Chem. Phys. 69*, 1352–1360.

Fairclough, R., & Cantor, C. R. (1978) *Methods Enzymol. 48*, 347–379.

Haas, E., Wilchek, M., Katchalski-Katzir, E., & Steinberg, I. Z. (1975) *Proc. Natl. Acad. Sci. U.S.A. 72*, 1807–1811.

Haas, E., Katchalski-Katzir, E., & Steinberg, I. Z. (1978) *Biochemistry 17*, 5064–5070.

Haas, E., McWherter, C. A., & Scheraga, H. A. (1988) *Biopolymers 27*, 1–21.
Hahn, L. H. E., & Hammes, G. G. (1978) *Biochemistry 17*, 2423–2429.
Hillel, Z., & Wu, C. W. (1976) *Biochemistry 15*, 2105–2113.
Lakowicz, J. R., Gryczynski, I., Cheung, H. C., Wang, C. K., Johnson, M. L., & Joshi, N. (1988) *Biochemistry 27*, 9149–9160.
Lakowicz, J. R., Gryczynski, I., Wiczk, W., Laczko, G., Prendergast, F. C., & Johnson, M. L. (1990a) *Biophys. Chem. 36*, 99–115.
Lakowicz, J. R., Kusba, J., Wiczk, W., Gryczynski, I., & Johnson, M. L. (1990b) *Chem. Phys. Lett. 193*, 319–326.
Martinez, M. C. L., & Garcia de la Torre, J. (1987) *Biophys. J. 52*, 303–310.
Rice, K. G., Wu, P. G., Brand, L., & Lee, Y. C. (1991) *Biochemistry 30*, 6646–55.
Riddles, P. W., Blakeley, R. L., & Zerner, B. (1979) *Anal. Biochem. 94*, 75–81.
Steiner, R. F. (1990) *Comments Mol. Cell. Biophys. 6*, 383–404.
Steiner, R. F., Albaugh, A., & Kilhoffer, M. (1991) *J. Fluoresc. 1*, 15–22.
Stryer, L. (1978) *Annu. Rev. Biochem. 47*, 819–846.
Wu, P. G., Rice, K. G., Lee, Y. C., & Brand, L. (1991) *Proc. Natl. Acad. Sci. U.S.A. 88*, 9355–9359.